King Saud University

Arabian Journal of Chemistry

www.ksu.edu.sa
www.sciencedirect.com

ORIGINAL ARTICLE

Electrochemical preparation of a novel type of C-dots/ZrO$_2$ nanocomposite onto glassy carbon electrode for detection of organophosphorus pesticide

Puthalapattu ReddyPrasad [a], **Eliazer Bobby Naidoo** [a],
Neelam Yugandhar Sreedhar [b,*]

[a] *Department of Chemistry, Vaal University of Technology, P. Bag X021, Vanderbiljpark 1900, South Africa*
[b] *Department of Chemistry, Electroanalytical lab, Sri Venkateswara University, Tirupati, A.P, India*

Abstract A selective, sensitive novel electrochemical sensor for detection of methyl parathion on the preparation of a carbon dots (C-dots)/ZrO$_2$ nanocomposite was developed. The C-dots/ZrO$_2$ nanocomposite was fabricated using electrochemical deposition onto a glassy carbon electrode and characterized by scanning electron microscopy, transmission electron microscopy, X-ray diffraction, X-ray photoelectron spectroscopy and cyclic voltammetry. The optimum parameters such as effect of pH, accumulation time, accumulation potential, scan rate, effect of amount of C-dots and effect of amount of ZrO$_2$ were investigated. The C-dots/ZrO$_2$ modified glassy carbon electrode allowed rapid, selective determination of methyl parathion in rice samples by adsorptive stripping voltammetry. The stripping response was highly linear over the methyl parathion concentrations ranging from 0.2 ng mL^{-1} to 48 ng mL^{-1}, with a detection limit of 0.056 ng mL^{-1}. This novel electrochemical nanocomposite-based electrochemical sensor was successfully applied for the detection of methyl parathion in rice samples.

* Corresponding author. Tel.: +91 8772249666(303).
  E-mail address: sreedhar_ny@rediffmail.com (N.Y. Sreedhar).

1. Introduction

Parathion (Fig. 1) is one of the most commonly used organophosphorus pesticides. It is widely used in agriculture due to its high toxicity to insects and limited persistence in the environment. However, this use has resulted in a serious risk to human health and the environment (Gilliom et al., 1999; Vermeire et al., 2003). Many efforts have been made to develop sensitive, convenient and effective methods for

Figure 1   Structure of methyl parathion.

organophosphorus pesticide residue analysis in environmental and other samples (Jenkins et al., 2001; Russell et al., 2003). Analysis of organophosphorus pesticides in environmental and biological samples is routinely conducted using different analytical techniques such as gas chromatography (Bergh et al., 2010), GC–Mass Spectrometry (Steiner et al., 2005) and high performance liquid chromatography (Pinto et al., 1995). Hence, they are commonly used methods to successfully detect organophosphorus pesticide residues in real samples with high selectivity, sufficient sensitivity and precision. However, these methods require highly skilled personnel, specially equipped laboratories, and expensive chemicals which limit their extensive application in screening determination of organophosphorus pesticide residues (Min et al., 2007; Zhang et al., 2006). The electroanalytical techniques are proved to be very selective, sensitive for the determination of organic molecules, including pesticides, drugs and related molecules in various samples (Sreedhar et al., 2010; Reddy et al., 2013). These methods are faster, easier to be operated and more economic than spectroscopic and chromatographic methods.

Carbon-based materials have drawn increasing attention in recent years owing to exceptional advantages such as high optical absorptivity, chemical stability, biocompatibility and low toxicity (Li, 2012; Baker, 2010; Cao, 2013). These materials primarily include C-dots (Zhai et al., 2012; Pan et al., 2010), nanodiamonds (Krueger, 2008), carbon nanotubes (Welsher et al., 2009), fullerene (Jeong et al., 2009), and graphene (Gupta et al., 2011; Zhu et al., 2012; Zhuo et al., 2012). Among all of these materials, C-dots have drawn the most extensive notice, owing to their early discovery and adjustable parameters. However, many scientific issues with C-dots still await further investigation. Zirconia (ZrO_2) is a crystalline inorganic oxide with thermal stability, chemical inertness, and a lack of toxicity (Pomfret et al., 2005; Valot et al., 1997). It has a strong affinity to phosphoric moieties and was originally reported for the detection of phosphopeptide enrichment (Hoang et al., 2010), phosphoprotein capture (Wang et al., 2009; Liu et al., 2008) and organophosphorus pesticides (Du et al., 2008). In this paper, a novel C-dots/ZrO_2 nanocomposite was electrochemically deposited on a glassy carbon electrode (GCE) for electrochemical detection of nitroaromatic organophosphorus pesticides. The C-dots/ZrO_2 nanocomposite was homogeneously dispersed on the surface of glassy carbon electrode. The intercalation also increases the contact area between the ZrO_2 and the C-dots, and therefore allows for more efficient electron transfer. The results are compared with C-dots, ZrO_2 modified electrodes and C-dot/ZrO_2 nanocomposite modified electrode and the latter was found to be more sensitive and selective to methyl parathion due to a synergistic effect. The improved performance combines the advantages of a large surface area and the fast electron-transfer of C-dots with the strong affinity of

ZrO_2 to the phosphate group. This further opens new opportunities for a facile, selective and rapid analysis of methylparathion in rice samples by adsorptive stripping voltammetry (AdSV). Meanwhile nitroaromatic organophosphorus pesticides such as methyl parathion, dicapthon, paraoxon and fenitrothion exhibit good redox behaviors at the modified electrode surface.

2. Experimental

2.1. Reagents and apparatus

Methyl parathion, zirconium oxychloride ($ZrOCl_2$), sodium borohydride ($NaBH_4$), phosphate buffer solution (PBS) and acetate buffer were purchased from Sigma–Aldrich, whereas glucose from Merck Chemicals. All stock and buffer solutions were prepared with double distilled water. Electrochemical measurements were performed on a Autolab PGSTAT 101 supplied by Metrohm, the Netherlands, with a conventional three-electrode system comprised of platinum wire as the auxiliary electrode, Ag/AgCl as the reference, a C-dots, ZrO_2 and C-dots/ZrO_2 modified glass carbon electrode (C-dots/ZrO_2/GCE) as the working electrode. X-ray photoelectron spectroscopy (XPS) analysis was carried out on an ESCALAB MK II X-ray photoelectron spectrometer. Peak positions were compared with the standard pattern to identify the crystalline phase. Raman spectra were collected on an HR 800 Raman spectroscopy (J Y, France) equipped with synapse a confocal Olympus microscope. X-ray diffraction (XRD) patterns were obtained using a Philips Xpert X-ray diffractometer using Cu Ka radiation at $\lambda = 1.5418$ Å. Transmission electron microscopy (TEM) micrographs were performed by JEOL 2000 transmission electron microscopy operating at 200 KV. The morphology of electrochemical nanocomposite was examined using a JEOL JSM-6701F scanning electron microscope (SEM). Measurements of UV-vis absorption and fluorescence spectra were carried out with Shimadzu UV-2200 and Hitachi F-7000 spectrophotometers, respectively. Elico Li-129 Model glass calomel combined-electrode was employed for measuring pH values.

2.2. Preparation of C-dots

A Suitable amount of glucose was dissolved in ultrapure water (50 mL) to form a clear solution (1 mol L^{-1}). 4.0 g of NaOH (50 mL) solution was added to the solution of glucose, then the mixed solution was treated by an ultrasonic wave (150 W, 40 KHz) for 1.2 h. The unfinished sample obtained from glucose/NaOH was adjusted to pH 7.0 with hydrochloric acid (2 mol L^{-1}). Subsequently, the crude solution was given a dialysis treatment using a semipermeable membrane (MWCO 1000) to remove any impurities except for the C-dots sample. After filter treatment, the obtained solution was brown, implying the formation of C-dots.

2.3. Preparation of C-dots/ZrO₂ nanocomposite modified electrode

Prior to electrodeposition, the GCE was polished carefully to a mirror-like finish with 0.3 and 0.05 μm alumina powder slurry and sonicated in double-distilled water and anhydrous ethanol

sequentially. The electrochemical deposition of graphitic like C-dots was performed on the Autolab PGSTAT 101 electrochemical station with a three-electrode system as described above by direct cyclic voltammetric electrolysis in 0.3 mg mL^{-1} dispersion under magnetic stirring with nitrogen bubbling. For the preparation of the C-dots and ZrO_2 nanocomposite modified GCE (C-dots/ZrO_2/GCE), the $ZrOCl_2$ (2.0 mg mL^{-1}) and C-dots (0.3 mg mL^{-1}) were added to a 1.2 ml of 0.05% chitosan solution. The above solution sonicated thoroughly until a homogenous suspension was obtained. This solution was deposited onto the GCE by cyclic voltammetry between −1.2 and +0.8 V at a scan rate of 50 mV s^{-1} for 5 successive scans.

The C-dots/ZrO_2/GCE was immersed into a stirred sample solution containing the desired concentration of methyl parathion for a given time. The enriched methyl parathion modified C-dots/ZrO_2/GCE was transferred into an acetate buffer (pH 4.0) solution for AdSV measurements. Prior to each electrochemical measurement, the electrolyte solution was purged with N_2 for 300 s.
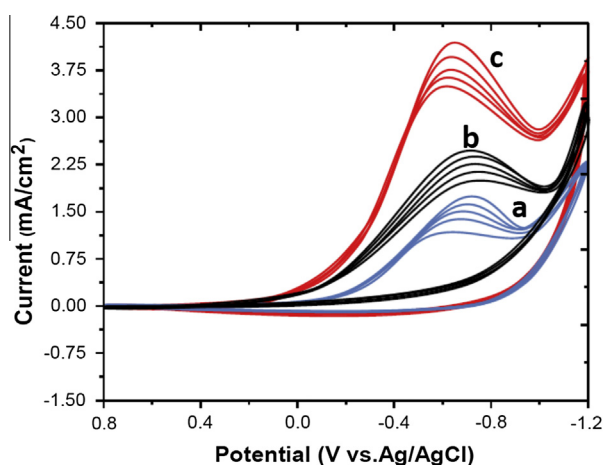
Figure 2 Cyclic voltammograms of electrochemical deposition process of (a) C-dots/GCE, (b) ZrO_2/GCE, (c) C-dots/ZrO_2/GCE at acetate buffer (pH: 4.0), concentration methyl parathion: 5.0 ng mL^{-1}, accumulation time: 140 s, accumulation potential; −0.8 V, scan rate: 50 mV s^{-1}.
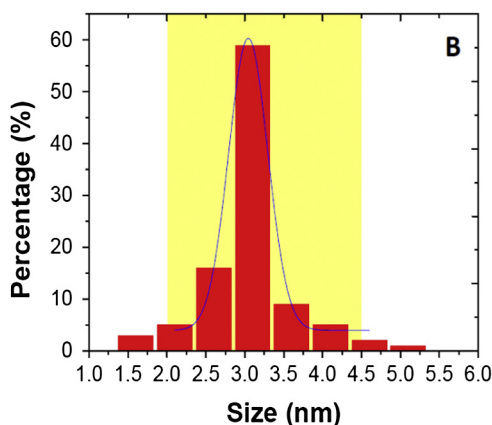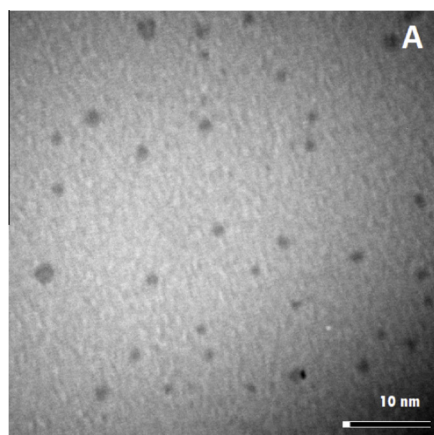
2.4. Electrochemical deposition of C-dots/ZrO_2 nanocomposite

Fig. 2, shows the cyclic voltammograms of the electrodeposition processes of C-dots (peaks a), ZrO_2 (peaks b) and C-dots/ZrO_2 (peaks c) on pretreated GCE. The steep rise in the peak currents of C-dots/ZrO_2 corresponds to the redox behavior of C-dots and ZrO_2 on the electrode. Corresponding redox behavior could also be observed in each C-dots or ZrO_2 modified electrode. In order to explore the surface properties of the modified electrodes, $K_3[Fe(CN)_6]$ was used to investigate the electroactive area of diverse electrodes. The redox peak currents of $K_3[Fe(CN)_6]$ increased at C-dots/ZrO_2/GCE. According to Randles–Sevcik equation, $Ip = 2.69 \times 10^5 \times n^{3/2} AD_0^{1/2} C_0 v^{1/2}$, where n is the number of electrons involved ($n = 1$; in the $[Fe(CN)_6]^{3-/4-}$ redox system), A is the geometric area of the electrode (0.14 cm^2), D is the diffusion coefficient of the $[Fe(CN)_6]^{3-/4-}$ and C is the concentration of $[Fe(CN)_6]^{3-}$, and the electroactive area (A) could be determined from cyclic voltammograms (Da-Jung et al., 2012). The electroactive area of diverse electrodes of C-dots (peaks a), ZrO_2 (peaks b) and C-dots/ZrO_2 (peaks c) is 0.56, 0.88, 1.20 cm^2, respectively. Noticeably, the C-dots/ZrO_2 modified electrode increased the electroactive surface area significantly larger than that of the C-dots and bare electrode respectively. The enhanced surface contributes to adsorbing more methyl parathion and thereby improving the detection sensitivity.

3. Results and discussion

In our experiment, a facile and one-step ultrasonic synthetic itinerary was employed for the synthesis of C-dots from glucose. The morphology and structure of graphitic like C-dots were confirmed by UV–vis, Fluorescence spectroscopy, TEM and Raman spectroscopy. Fig. 3A, shows the TEM images of the C-dots, which can be seen to have a uniform dispersion without apparent aggregation and the corresponding dot size distribution histogram obtained by counting about 60 dots indicates that these dots have size 3–3.2 nm (Fig. 3B). Fig. S1, shows the UV–vis absorption and photoluminescence (PL) emission spectra of the aqueous dispersion of the C-dots. The UV–vis absorption spectra of C-dots in water show an absorption band at 342 nm attributed to the Π–Π^* transition.

Figure 3 (A) TEM images and (B) corresponding C-dots size distribution histogram of the nanocomposite.

The C-dots dispersion shows a strong PL emission peak centered at 446 nm when excited at 360 nm, indicating that the C-dots are fluorescent. Insets of Fig. S1, show the photograph
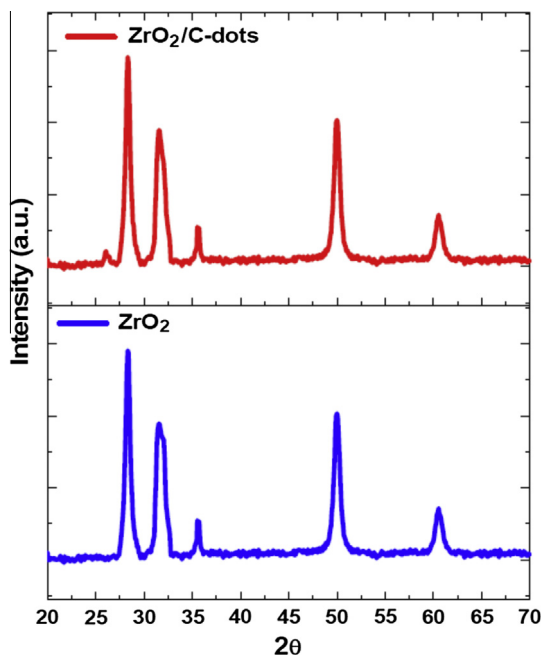

Figure 4   XRD pattern of the obtained ZrO_2 and C-dots/ZrO_2.

of the water-dispersed C-dots illuminated under 365 nm UV light. It shows bluish green fluorescence color can be observed by exposed eye, which is similar to the graphene quantum dots and probably attributable to their small size and surface states. Fig. S2, shows the Raman spectra of C-dots of two characteristic peaks observed at 1336 and 1605 cm^{-1} are corresponding to the D-band and G-band, which is similar to the graphene structure. The above observations confirmed the formation of graphitic like C-dots from glucose.

X-ray diffraction patterns in Fig. 4 give further support to different crystalline structures of the formation of as-electrodeposited nanocomposites. The formation of ZrO_2 nanocomposite shows strong peaks at 28.6, 31.6, 35.6, 50.4 and 60.0 were obvious, which is in good agreement with the standard data for JCPDC no. 79-1771. For the C-dots/ZrO_2 nanocomposite, a new diffraction peak centered at 26.2°, indicating that the graphitic like C-dots were present in the modified electrode. There was a small deviation resulting from the interactions between C-dots and ZrO_2 and no peaks of any other phases or impurities were detected in this pattern. The TEM image of the ZrO_2 and C-dots/ZrO_2 nanocomposites exhibited a typical spherical like structure with thin layer coating as shown in Fig. 5A and C. Fig. 5A reveals that the spherical particles of ZrO_2 are mainly uniform dispersion with relatively thin width and about 15–20 nm in size. In Fig. 5C, they show well coated surface of C-dots/ZrO_2 on GCE. Additionally, the morphology of nanocomposite was further investigated by SEM. From SEM images of the ZrO_2 (Fig. 3B) and C-dots/ZrO_2

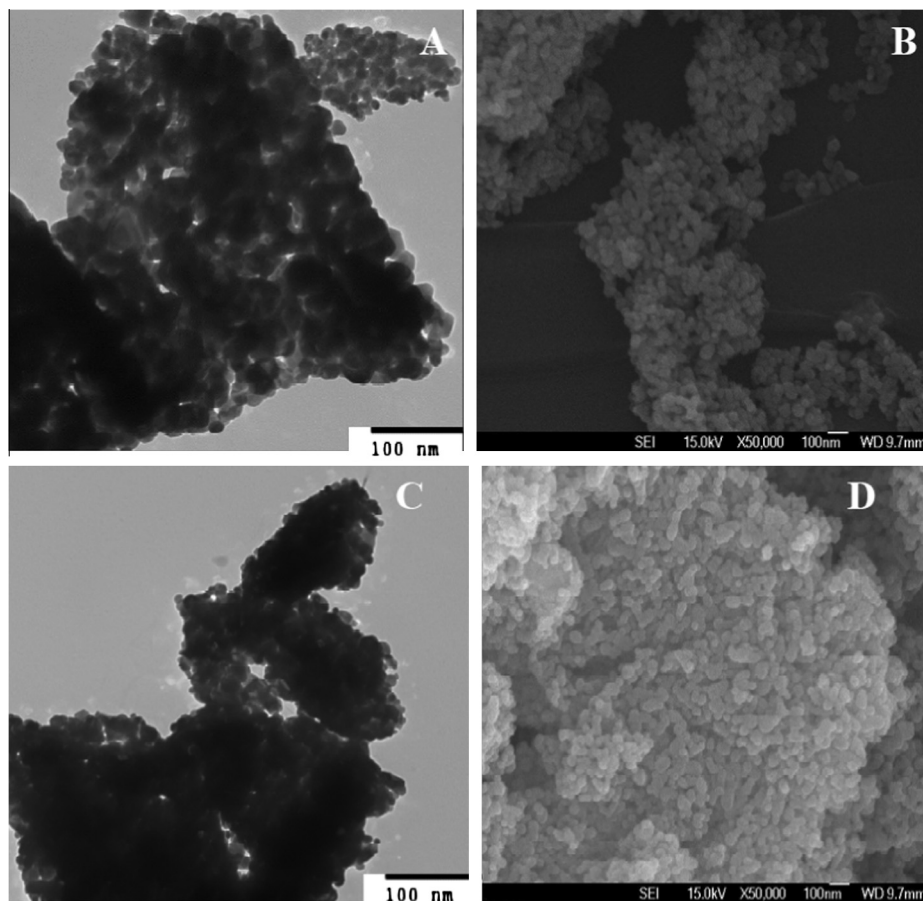**Figure 5**   TEM images of fabricated (A) ZrO_2 (C) C-dots/ZrO_2 and SEM image of (B) ZrO_2 (D) C-dots/ZrO_2 nanocomposites.

(Fig. 5D) nanocomposites which were electrochemically deposited on the electrode surface, it can be seen that the well-packed C-dots/ZrO$_2$ nanocomposite was displayed. Therefore, the effective adsorption of methyl parathion and the fast electron transfer rate may benefit from the nanostructured C-dots/ZrO$_2$ nanocomposite. The C-dots and modified C-dots/ZrO$_2$ were further characterized by XPS, which is effective at observing the inner structure of carbon for carbon-based materials. The two peaks at 284.6 and 531.6 eV shown in the XPS spectrum (Fig. 6A) of these C-dots are attributed to C1s and O1s, respectively. Fig. 6A, shows that the bands centered at 181.6, 284.8 and 531.6 eV are associated with Zr3d, C1s and O1s, respectively. It is clearly seen that the Zr3d spectra of C-dots/ZrO$_2$ nanocomposite are the existence of ZrO$_2$ nanoparticles in C-dots/ZrO$_2$ nanocomposite after the one-step electrochemical deposition. The C1s XPS spectrum of C-dots shows some oxygen functionalities as C-dots (Fig. 6B), while the absorbance peaks of C-dots at 284.3, 285.2 and 287.8 eV, correspond to C—C, C—O and C=O/COOH, respectively. Moreover, the O1s spectrum shows two peaks at 531.2 and 532.2 eV (Fig. 6C), which are attributed to C—O and C=O, respectively. These results indicate that C-dots were formed with some oxygen functionalities. Consequently, the presence of active groups of C-dots such as carbonyl and hydroxyl acts as the nucleation, growth sites for ZrO$_2$ and extends the surface area and lifetime of the electrochemical nanocomposite of C-dots/ZrO$_2$. All these results illustrate that the Zr3d spectra of C-dot/ZrO$_2$ nanocomposite were obvious compared to that of C-dots, indicating the existence of ZrO$_2$ nanoparticles in C-dot/ZrO$_2$ nanocomposite after the one-step electrochemical deposition.

3.1. Electrochemical behavior of the adsorbed methyl parathion on modified electrode

From Fig. 7 (peak c), the incubating C-dots/ZrO$_2$/GCE in 10 ng mL^{-1} methyl parathion for 5 min, the resulting methyl parathion/C-dots/ZrO$_2$/GCE displayed well-defined redox peaks (E_{pa} = 0.085 V, E_{pc} = −0.82 V) and an irreversible reduction peak (E_{pa} = 0.16 V). When replacing the C-dots-ZrO$_2$/GCE with ZrO$_2$/GCE or C-dots/GCE as the working electrode to enrich 5.0 ng mL^{-1} of methyl parathion, both the resulting methyl parathion/C-dots/GCE (peak a) and methyl parathion-ZrO$_2$/GCE (peak b) also displayed three peaks in an acetate buffer at pH 4.0. However, they were obviously smaller than that of C-dots/ZrO$_2$/GCE. It is not surprising that the C-dots/ZrO$_2$, combining C-dots and ZrO$_2$ nanoparticles, enhanced the detection signal more than an individual C-dots or ZrO$_2$ due to a synergistic effect. In comparison with the methyl parathion responses on different electrodes, the methyl parathion/C-dots/GCE (peak a) and methyl parathion-ZrO$_2$/GCE (peak b), methyl parathion/C-dots/ZrO$_2$/GCE (peak c) resulted in an obvious reduction peak at -0.82 V in acetate buffer at pH 4.0. Thus, the maximum response was observed at methyl parathion/C-dots/ZrO$_2$/GCE, which was consistent with the cyclic voltammetry measurements. Consequently, the anodic peak currents increased with an increase in the scan rate and were proportional to the
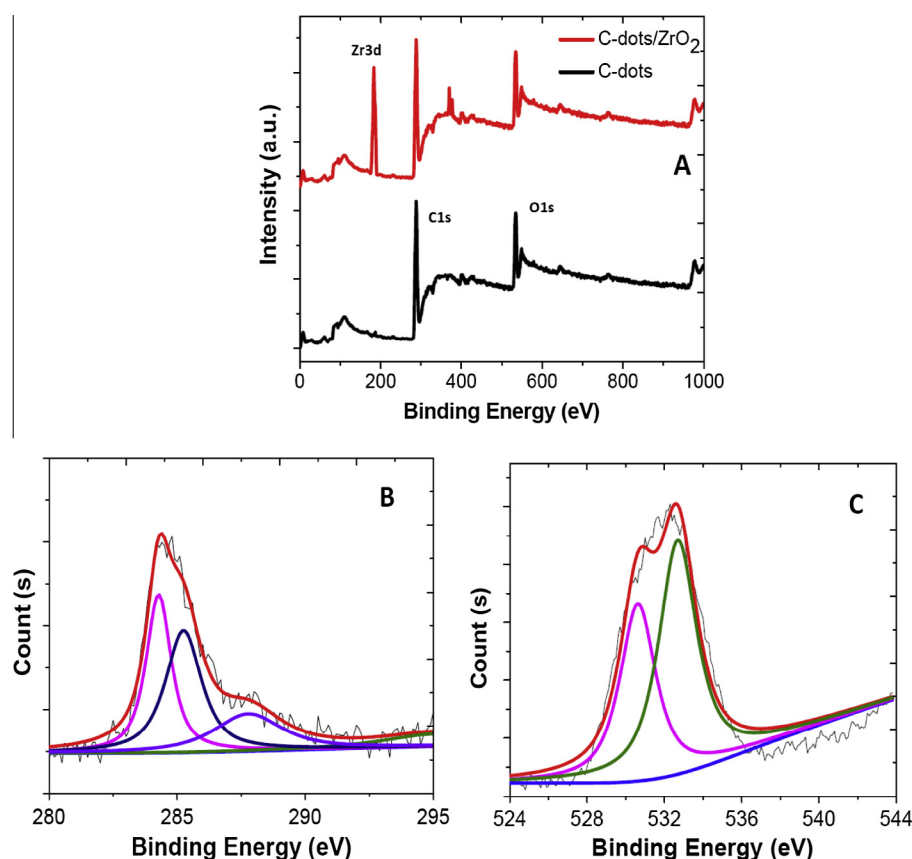

**Figure 6** (A) XPS spectra of C-dots, C-dots/ZrO$_2$, (B) C$_{1S}$, (C) O$_{1S}$ XPS spectra of C-dots.

scan rate in the range from 10 to 200 mV s^{-1} (Fig. 8) suggesting that the electrode reaction of the immobilized methyl parathion is a surface controlled process and the correlation coefficient (R^2) 0.9907 ($y = 0.0198x + 3.0988$). The irreversible reduction peak corresponds to the reduction of the nitro group to the hydroxylamine group (Liu and Lin., 2005) and the reversible redox peaks are attributed to a four electron-transfer processes of nitroso group. The electrochemical mechanism is shown in Fig. S3.

3.2. Effect of C-dots and ZrO$_2$ nanocomposites

Fig. 9, shows the concentration of C-dots for detection of methyl parathion. The AdSV currents increased with increasing the content of C-dots in the deposition solution
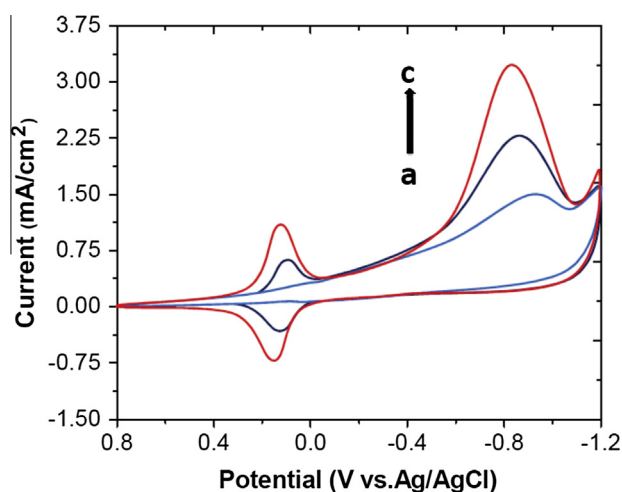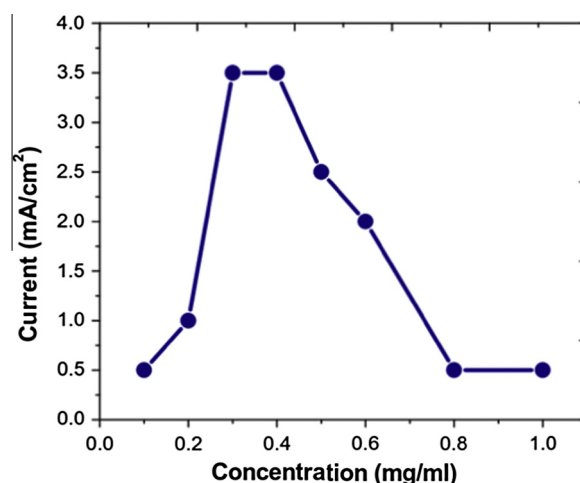
Figure 7 Cyclic voltammograms of methyl parathion at (a) C-dots/GCE, (b) ZrO$_2$/GCE, (c) C-dots/ZrO$_2$/GCE at acetate buffer (pH: 4.0), concentration of methyl parathion: 5.0 ng mL^{-1}; accumulation potential; −0.8 V, accumulation time: 140 s, scan rate: 50 mV s^{-1}.
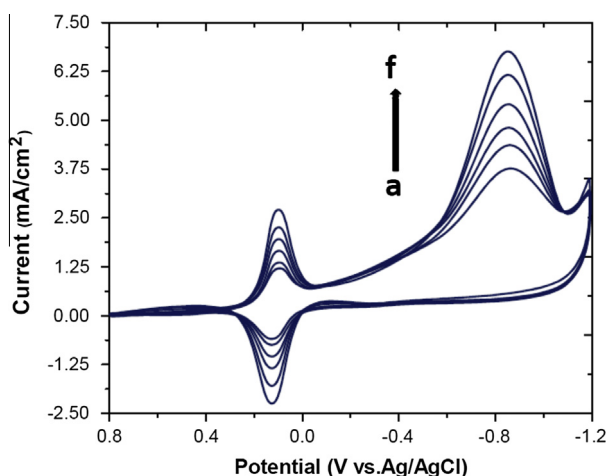
Figure 8 Cyclic voltammograms at C-dots/ZrO$_2$/GCE in a 0.1 M acetate buffer (pH: 4.0) at various scan rates: (a) 20, (b) 50, (c) 75, (d) 100, (e) 150, (f) 200 mV s^{-1} of methyl parathion, instrument: AdSV, concentration of methyl parathion: 5.0 ng mL^{-1}, accumulation potential; −0.8 V, accumulation time: 140 s, scan rate: 50 mV s^{-1}.

and reached a maximum at 0.3 mg mL^{-1} C-dots. The sp^2-hybridized structure may contribute to the high capacitance value, particularly for C-dots, and result in high background current as reported earlier (da Silva et al., 2014). The decrease in current at a higher concentration of C-dots may be attributed to an increase in the electrode capacitance, which introduces high background current and decreases the sensitivity of the stripping response. As a result, 0.3 mg mL^{-1} C-dots were used to prepare on GCE surface. The amount of ZrO$_2$ was another influence on the methyl parathion adsorption and detection sensitivity. Fig. 10, showed that the voltammetric currents are affected by the different concentrations of ZrOCl$_2$ used during the one-step electrodeposition of C-dots/ZrO$_2$ on GCE to enrich methyl parathion. The response current increased upon raising the concentration of ZrOCl$_2$ and then decreased after reaching 2.0 mg mL^{-1} ZrOCl$_2$ in the deposition solution. It was found that a high

Figure 9 Effects of the content of C-dots in the deposition solution on GCE, instrument: AdSV, acetate buffer (pH 4.0), concentration of methyl parathion: 5.0 ng mL^{-1}; accumulation potential; −0.8 V, accumulation time: 140 s, scan rate: 50 mV s^{-1}.
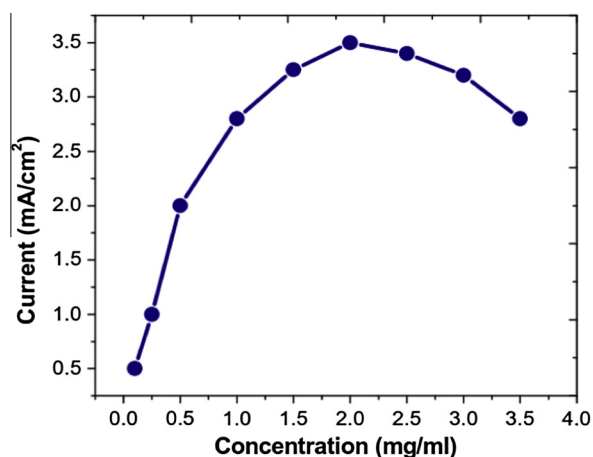
**Figure 10** Effect of the amount of ZrO$_2$ nanoparticles on GCE, instrument: AdSV, acetate buffer (pH 4.0), concentration of methyl parathion: 5.0 ng mL^{-1}; accumulation potential; −0.8 V, accumulation time: 140 s, scan rate: 50 mV s^{-1}.

concentration of $ZrOCl_2$ (>2 mg mL^{-1}) caused the heavy aggregation of ZrO_2 nanoparticles. Thus, 2.0 mg mL^{-1} $ZrOCl_2$ was used in the preparation of C-dots /ZrO_2/GCE.
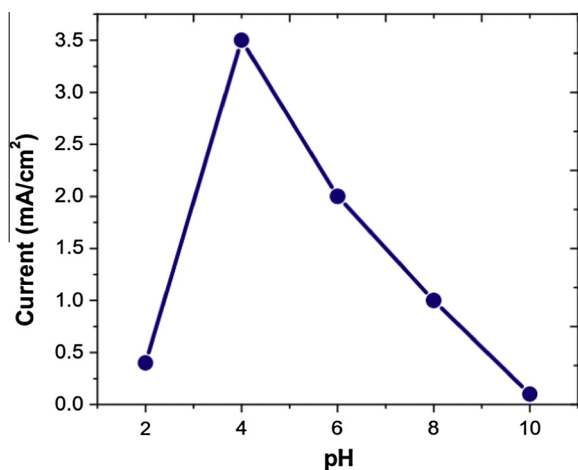
Figure 11   Effect of pH for methyl parathion reduction peak current at acetate buffer, instrument: AdSV, accumulation potential: -0.8 V, accumulation time: 140 s, concentration of methyl parathion: 5.0 ng mL^{-1}, scan rate: 50 mVs^{-1}.
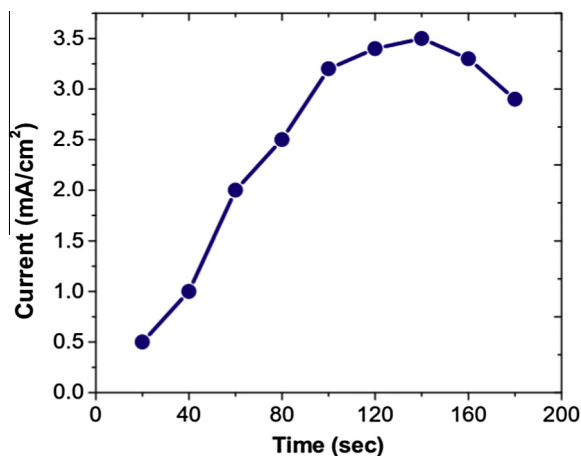
Figure 12   The effect of adsorption time on the stripping currents of methyl parathion at acetate buffer (pH 4.0), instrument: AdSV, accumulation potential: -0.8 V, concentration of methyl parathion: 5.0 ng mL^{-1}, scan rate: 50 mV s^{-1}.

Table 1   Determination of methyl parathion in rice samples.

| Sample	Spiked amount (ng mL^{-1})	Found[*] (ng mL^{-1})	Recovery (%)	SD	RSD (%)
Rice	5.0	4.99	99.80	0.050	0.08
	10.0	9.98	99.80	0.022	0.12
	20.0	20.00	100.00	0.028	0.04
	40.0	39.97	99.92	0.003	0.06

[*] Average of six determinations ± standard deviation.

3.3. Effect of pH and adsorption time

The pH was one of the important optimized parameters for detection of methyl parathion for measurement of the voltammetric response. We observed that the stripping signal increased with an increase of pH up to 4 and then decreased at higher pH (Fig. 11), which might be due to the degradation of methyl parathion in basic media. To achieve the highest signal, pH 4 acetate buffer was used in the measurements. The stripping current responses also depended on the adsorption time of methyl parathion. It was found that the stripping responses increased with increasing adsorption time and tended to reach a high value at 140 s (Fig. 12). The rapid and highly effective enrichment of methyl parathion was attributed to the strong affinity of C-dots/ZrO_2 to nitroaromatic compounds.
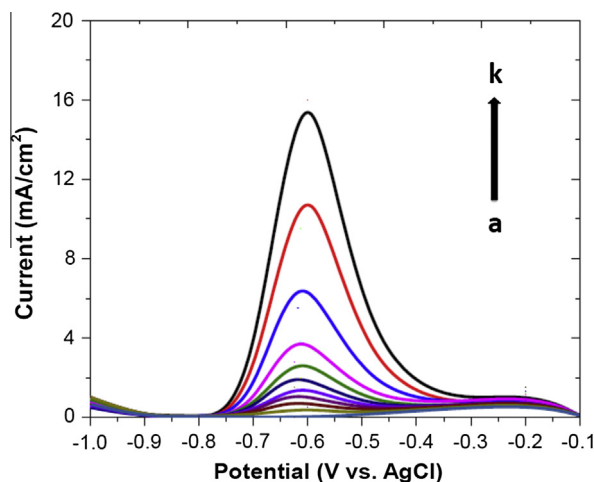
Figure 13   Adsorptive stripping voltammograms at C-dots/ZrO_2/GCE in a 0.1 M acetate buffer (pH: 4.0) at various concentrations: (a) blank, (b) 0.2, (c) 0.4, (d) 0.8, (e) 1.0, (f) 2.0, (g) 4.0, (h) 8.0, (i) 16.0, (j) 32.0, (k) 48.0 (ng mL^{-1}) of methyl parathion, scan rate: 50 mV s^{-1}.
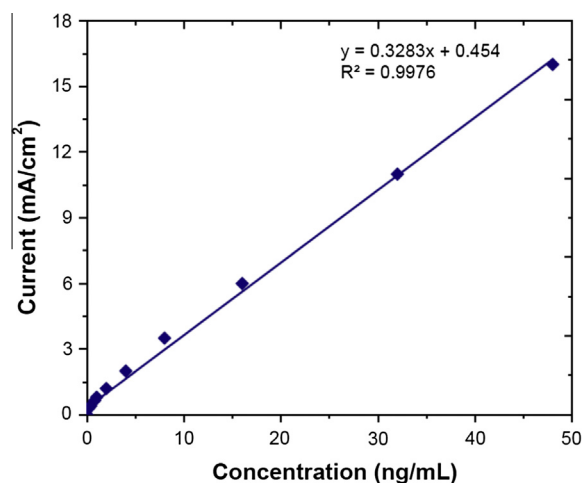
Figure 14   Linear plot for methyl parathion, other variable conditions are same as in Fig. 13.

The influence of accumulation potential is examined from -0.8 to $+0.7$ V. Based on the results the peak current of methyl parathion is almost independent of accumulation potential. This is due to the neutral nature of methyl parathion under this condition.

3.4. Determination of methyl parathion and analytical performance

The reliability of the proposed adsorptive stripping voltammetry method for the determination of methyl parathion was investigated by assaying this pesticide in rice sample. A series of methyl parathion rice samples were used to further investigate the accuracy of the proposed method. The rice samples are sprayed with spiking different amounts of methyl parathion with known concentrations and left for 2–4 h. After that, it is extracted with acetone (2×50 ml) by shaking the flask for 10 min. The organic phase is filtered under suction through Whatman No. 1 filter paper. The solvent was removed through evaporation and the residues of the compounds were dissolved in ethanol and transferred into volumetric flask. The results were summarized in Table 1. The recoveries were in the range of 99.80–100.0%, indicating that the proposed method was highly accurate and can be directly used for real-life sample detection.

Under optimal experimental conditions, the C-dots/ZrO_2/GCE was examined with different concentrations of methyl parathion as shown in Fig. 13. That well-defined AdSV responses from adsorbed methyl parathion were observed and increased with an increase in methyl parathion concentration. The resulting calibration plot of stripping currents vs. concentrations was linear over 0.2 ng mL^{-1} to 48 ng mL^{-1} of methyl parathion (Fig. 14), with the linear regression equation of I (μA) $= 0.3283$ (ng mL^{-1}) $+ 0.454$ with a correlation

coefficient (r): 0.9976. A detection limit of 0.056 ng mL^{-1} ($n = 6$) was obtained based on a signal-to-noise ratio of 3. It is much lower than that of the 5 ng mL^{-1} at the ZrO_2 modified electrode. The comparison of this method with other modified electrode nanocomposites for detection of methyl parathion is shown in Table 2. It indicated that the C-dots/ZrO_2 nanocomposite was more facile and selective in comparison with the detection limit values.

The adsorptive stripping voltammetric determination of methyl parathion was tested in the presence of spiked known amounts of interfering ions and molecules. Foreign ions arising from other electroactive nitrophenyl derivatives such as nitrobenzene, nitrophenol and oxygen-containing inorganic ions did not interfere with the detection of methyl parathion in rice samples. The tolerance limit was defined as the amount of the foreign substance causing a change of $\pm 2\%$ in the peak current intensity reading. The tolerable limits of interfering substance are given in Table 3.

The high selectivity is likely due to the strong affinity between C-dots/ZrO_2/GCE and methyl parathion. The adsorptive stripping potential is relatively negative (approximately -0.82 V), which also avoids the interferences from other phenol species and electroactive substances. For validation of the proposed method, various parameters, such as stability of the electrode, repeatability and reproducibility were evaluated in the determination of methyl parathion. The stability of C-dots/ZrO_2 modified GCE was tested by recording the AdSV response of 10 ng mL^{-1} methyl parathion on the modified electrode stored in room temperature several hours. The results indicated that the response of the C-dots/ZrO_2/GCE to methyl parathion slightly decreased after 10 days (10–15%), demonstrating the good stability of the modified electrode. To ascertain the repeatability of the method, 10 ng mL^{-1} methyl

Table 2 The relevant information of some reported methods for determination of organophosphorus pesticides.

Sensors	Substrate	Pesticides	Matrix	DL (ng mL^{-1})	Ref.
AuNPs	–	Methamidophos	Chinese cabbage	1.4	Li et al. (2011)
Mn:ZnSe dots	–	Paraoxon	Tap water	4.0	Gao et al. (2012)
Poly(3-hexylthiophene)/TiO$_2$ Nanoparticle	GCE	Chlorpyrifos	Green vegetables	3.51	Hongbo et al. (2011)
ZrO$_2$	Au electrode	Methyl parathion		3	Liu and Lin. (2005)
Au/ZrO2/SiO$_2$	GCE	Paraoxon-ethyl	–	0.5	Yang et al. (2012)
Au, CdS@ZnS QD	Test strip	TCP	Human saliva	0.47	Zhang et al. (2013)
C-dots/ZrO$_2$	GCE	Methyl parathion	Rice	0.14	Present work

Table 3 Effect of foreign species limit of interfering substances on AdSV determination of methyl parathion (5.0 ng mL^{-1}) using C-dots/ZrO$_2$/GCE; conditions: acetate buffer (pH 4.0); accumulation time: 140 s; accumulation potential: -0.80 V; scan rate: 50 mV s^{-1}.

Foreign species	Tolerance limit (μg mL^{-1})[a]
Pyrethroid pesticides, Carbamate pesticides, atrazine	1000
Phorate	500
Malathion, dimethoate, Al^{3+}, Zn^{2+}, Co^{2+}, SO$_4^{2-}$, As(V)	100
Phenol	50
K$^+$, Na$^+$, Ba^{2+}, Ca^{2+}, NH$_4^+$, Mg^{2+}, Mn^{2+}, Cu^{2+}, Cr^{3+}, NO^{3-}, Cd^{2+}, Fe^{3+}, SO$_3^{2-}$, Fe^{2+}, NO^{2-}	20

[a] Tolerance limit causing $\pm 2\%$ variation in absorbance value.

parathion and the same electrode (renewed every time) were used several hours within a day. The relative standard deviation (RSD) of 1.2% for 6 times parallel detections suggested good repeatability and reproducibility of the C-dots/ZrO$_2$/GCE.

4. Conclusion

In this work, we have presented a novel C-dots/ZrO$_2$ nanocomposite-based electrochemical sensor for detection of nitroaromatic organophosphorous pesticides. The results showed that the electrochemical nanocomposite could rapidly and specifically determine methyl parathion in rice samples with a detection limit of 0.056 ng mL^{-1} under optimal conditions. The C-dots/ZrO$_2$ nanocomposite, when used as a capturing agent allows for the fast adsorption of the target analyte due to its strong affinity to phosphoric moieties and shows the fast electron-transfer kinetics, excellent electrocatalytic activity for electroactive species. The developed method shows great promise for in-field and point-of-care diagnosis of organophosphorous pesticide exposures, as well as further validation of the performance of these devices and fabrication of a viable and affordable disposable version.

Acknowledgment

Appendix A. Supplementary material

Supplementary data associated with this article can be found, in the online version, at http://dx.doi.org/10.1016/j.arabjc.2015.02.012.

References

Baker, S.N., Baker, G.A., 2010. Luminescent carbon nanodots: emergent nanolights. Angew. Chem. 122, 6876–6896.

Bergh, C., Torgrip, R., Ostman, C., 2010. Simultaneous selective detection of organophosphate and phthalate esters using gas chromatography with positive ion chemical ionization tandem mass spectrometry and its application to indoor air and dust. Rapid Commun Mass Spectrom. 24 (19), 2859–2867.

Cao, L., Meziani, M.J., Sahu, S., Sun, Y.P., 2013. Photoluminescence properties of graphene versus other carbon nanomaterials. Acc. Chem. Res. 46, 171–180.

da Silva, H., Pacheco, J.G., Magalhaes, J.M.C.S., Viswanathan, S., Delerue-Matos, C., 2014. MIP-graphene-modified glassy carbon electrode for the determination of trimethoprim. Biosens. Bioelectron. Biosens. Bioelectron. 52, 56–61.

Da-Jung, C., Oh, S., Komathi, S., Gopalan, A.I., Lee, K.P., Choi, S., 2012. One-step modification of various electrode surfaces using diazonium salt compounds and the application of this technology to electrochemical DNA (E-DNA) sensors. Electrochim. Acta 76, 394–403.

Du, D., Ye, X., Zhang, J., Zeng, Y., Tu, H., Zhang, A., Liu, D., 2008. Stripping voltammetric analysis of organophosphate pesticides based on solid-phase extraction at zirconia nanoparticles modified electrode. Electrochem. Commun. 10, 686–690.

Gao, X., Tang, G.C., Su, X.G., 2012. Optical detection of organophosphorus compoundsbased on Mn-doped ZnSe d-dot enzymatic catalytic sensor. Biosens. Bioelec-tron. 36, 75–80.

Gilliom, R.J.B., Barbash, J.E., Kolpin, D.W., Larson, S.J., 1999. Testing water quality for pesticide pollution. Environ. Sci. Technol. 33, 164A–169A.

Gupta, V., Chaudhary, N., Srivastava, R., Sharma, G.D., Bhardwaj, R., Chand, S., 2011. Luminscent graphene quantum dots for organic photovoltaic devices. J. Am. Chem. Soc. 133, 9960–9963.

Hoang, T., Roth, U., Kowalewski, K., Belisle, C., Steinert, K., Karas, M., 2010. Highly specific capture and direct MALDI MS analysis of phosphopeptides by zirconium phosphonate on self-assembled monolayers. Anal. Chem. 82, 219–228.

Hongbo, Li., Jing, Li., Qin, Xu., Xiaoya, Hu., 2011. Poly(3-hexylthiophene)/TiO$_2$ nanoparticle-functionalized electrodes for visible light and low potential photoelectrochemical sensing of organophosphorus pesticide chlopyrifos. Anal. Chem. 83, 96810–99686.

Jenkins, A.L., Yin, R., Jensen, J.L., 2001. Molecularly imprinted polymer sensors for pesticide and insecticide detection in water. Analyst 126, 798–802.

Jeong, J., Cho, M., Lim, Y.T., Song, N.W., Chung, B.H., 2009. Synthesis and characterization of a photoluminescent nanoparticle based on fullerene–silica hybridization. Angew. Chem. 121, 5400–5403.

Krueger, A., 2008. Diamond nanoparticles: jewels for chemistry and physics. Adv. Mater. 20, 2445–2449.

Li, H.K., Guo, J.J., Ping, H., Liu, L.R., Zhang, M.W., Guan, F.R., Sun, C.Y., Zhang, Q., 2011. Visual detection of organophosphorus pesticides represented by mathami-dophos using Au nanoparticles as colorimetric probe. Talanta 87, 93–99.

Li, H., Kang, Z., Liu, Y., Lee, S.T., 2012. Carbon nanodots: synthesis, properties and applications. J. Mater. Chem. 22, 24230–24253.

Liu, G., Lin, Y., 2005a. Electrochemical sensor for organophosphate pesticides and nerve agents using zirconia nanoparticles as selective sorbents. Anal. Chem. 77, 5894–5901.

Liu, G., Lin, Y., 2005b. Electrochemical stripping analysis of organophosphate pesticides and nerve agents. Electrochem. Commun. 7, 339–343.

Liu, G., Wang, J., Barry, R., Petersen, C., Timchalk, C., Gassman, P.L., Lin, Y., 2008. Nanoparticle-based electrochemical immunosensor for the detection of phosphorylated acetylcholinesterase: an exposure biomarker of organophosphate pesticides and nerve agents. Chem. Eur. J. 14, 9951–9959.

Min, H., QU, Y.H., Li, X.H., Xie, Z.H., Wei, Y.Y., Jin, L.T., 2007. Au-doped Fe$_3$O$_4$ nanoparticle immobilized acetylcholinesterase sensor for the detection of organophosphorus pesticide. Acta. Chim. Sinica 65, 2303–2308.

Pan, D., Zhang, J., Li, Z., Wu, C., Yan, X., Wu, M., 2010. Observation of pH, solvent, spin, and excitation-dependent blue photoluminescence from carbon nanoparticles. Chem. Commun. 46, 3681–3683.

Pinto, C.G., Perez Pavon, J.L., Cordero, B.M., 1995. Cloud point preconcentration and high-performance liquid chromatographic determination of organophosphorus pesticides with dual electrochemical detection. Anal. Chem. 67 (15), 2606–2612.

Pomfret, M.B., Stoltz, C., Varughese, B., Walker, R.A., 2005. Structural and compositional characterization of yttria stabilized zirconia (YSZ): evidence of surface stabilized. Anal. Chem. 77, 1791–1795.

Reddy, C.N., Prasad, P.R., Sreedhar, N.Y., 2013. Electrochemical analysis of anti chemotherapeutic drug zanosar in pharmaceutical and biological samples by differential pulse polarography. J. Anal. Meth. Chem. 1, 1–7.

Russell, A.J., Berberich, J.A., Drevon, G.E., Koepsel, R.R., 2003. Biomaterials for mediation of chemical and biological warfare agents. Annu. Rev. Biomed. Eng. 5, 1–27.

Sreedhar, N.Y., Sankara Nayak, M., Shashi Kumar, K.N., Srinivasa Prasad, K., Reddy Prasad, P., 2010. Stripping voltammetric determination of simeton in its formulations and vegetables. Environ. Monit. Assess. 170, 59–64.

Steiner, W.E., Klopsch, S.J., English, W.A., Clowers, B.H., Hill, H.H., 2005. Detection of a chemical warfare agent simulant in various aerosol matrixes by ion mobility time-of-flight mass spectrometry. Anal. Chem. 77, 4792–4799.

Valot, C., Ciosmak, D., Mesnier, M.T., Lallemant, M., 1997. Phase analysis by variable-incidence X-ray diffraction: application to zirconium oxidation. Oxid. Met. 48, 329–345.

Vermeire, T., MacPhail, R., Waters, M., 2003. Integrated human and ecological risk assessment: a case study of organophosphorous pesticides in the environment. Hum. Ecol. Risk. Assessment 9, 343–357.

Wang, H., Wang, J., Choi, D., Tang, Z., Wu, H., Lin, Y., 2009. EQCM immunoassay for phosphorylated acetylcholinesterase as a biomarker for organophosphate exposures based on selective zirconia adsorption and enzyme-catalytic precipitation. Biosens. Bioelectron. 24, 2377–2383.

Welsher, K., Liu, Z., Sherlock, S.P., Robinson, J.T., Chen, Z., Daranciang, D., Dai, H., 2009. A route to brightly fluorescent carbon nanotubes for near-infrared imaging in mice. Nat. Nanotechnol. 4, 773–780.

Yang, Y., Tu, H., Zhang, A., Du, D., Lin, Y., 2012. Preparation and characterization of Au–ZrO$_2$–SiO$_2$ nanocomposite spheres and their application in enrichment and detection of organophosphorus agents. J. Mater. Chem. 22, 4977–4981.

Zhai, X., Zhang, P., Liu, C., Bai, T., Li, W., Dai, L., Liu, W., 2012. Highly luminescent carbon nanodots by microwave-assisted pyrolysis. Chem. Commun. 48, 7955–7957.

Zhang, J., Wang, Y.L., Yuan, Z.B., 2006. Screen-printed enzyme electrodes for detection of organophosphate pesticide residue. Acta. Chim. Sinica 64, 428–434.

Zhang, W., Tang, Y., Du, D., Smith, J.N., Timchalk, C., Liu, D., Lin, Y., 2013. Direct analysis of trichloropyridinol in human saliva using an Au nanoparticles-based immunochromatographic test strip for biomonitoring of exposure to chlorpyrifos. Talanta 114, 261–267.

Zhu, S., Zhang, J., Liu, X., Li, B., Wang, X., Tang, S., Meng, Q., Li, Y., Shi, C., Hu, R., Yang, B., 2012. Graphene quantum dots with controllable surface oxidation, tunable fluorescence and up-conversion emission. RSC Adv. 2, 2717–2720.

Zhuo, S., Shao, M., Lee, S.T., 2012. Upconversion and downconversion fluorescent graphene quantum dots: ultrasonic preparation and photocatalysis. ACS Nano 6, 1059–1064.